ACADEMIC PRESS

Available online at www.sciencedirect.com
SCIENCE DIRECT®

NeuroImage

NeuroImage 20 (2003) 1639–1648

www.elsevier.com/locate/ynimg

Three-dimensional anatomical characterization of the developing mouse brain by diffusion tensor microimaging

Jiangyang Zhang,[a,b] Linda J. Richards,[c] Paul Yarowsky,[d] Hao Huang,[a,b] Peter C.M. van Zijl,[a,e] and Susumu Mori[a,e,*]

[a] *Johns Hopkins University School of Medicine, Department of Radiology, Division of NMR Research, 720 Rutland Ave., Baltimore, MD, 21205, USA*
[b] *Johns Hopkins University School of Medicine, Department of Biomedical Engineering, 720 Rutland Ave., Baltimore, MD, 21205, USA*
[c] *University of Maryland School of Medicine, Department of Anatomy and Neurobiology and The Program in Neuroscience, 685 W. Baltimore St., Baltimore, MD 21201, USA*
[d] *University of Maryland School of Medicine, Department of Pharmacology and Experimental Therapeutics and The Program in Neuroscience, 685 W. Baltimore St., Baltimore, MD 21201, USA*
[e] *F.M. Kirby Research Center for Functional Brain Imaging, Kennedy Krieger Institute, 707 North Broadway, Baltimore, MD 21205, USA*

Received 17 April 2003; revised 1 July 2003; accepted 3 July 2003

Abstract

Investigation of three-dimensional (3D) morphometry of developing brains has been hindered by a lack of imaging modalities that can monitor the 3D evolution of various anatomical structures without sectioning and staining processes. In this study, we combined magnetic resonance microimaging and diffusion tensor imaging techniques to accomplish such visualization. The application of this approach to developing mouse embryos revealed that it could clearly delineate early critical structures such as neuroepithelium, cortical plate, and various axonal structures, and follow their developmental evolution. The technique was applied to the study of the Netrin-1 mutant, allowing verification of its anatomical phenotype.

Introduction

Brain development consists of a cascade of complex, yet highly harmonized processes of neuronal cell proliferation, migration, and differentiation. These processes have been studied mostly with optical and electron microscopy, which can provide cellular level information, but spatially limited views. To study the dynamic three-dimensional (3D) process of the formation of brain structures, the development of 3D imaging techniques is essential. Although a number of such techniques exist (Johnson et al., 1993; Jacobs and Fraser, 1994; Boppart et al., 1996; Jacobs et al., 1999; Louie et al., 2000; Streicher et al., 2000; Sharpe et al., 2002; Weninger and Mohun, 2002), it has not been possible to discretely delineate early regions of the nervous system such as the neuroepithelium, cortical plate, and axonal organization without the use of brain sectioning and/or staining processes. Here, we show that magnetic resonance diffusion tensor microimaging (DTMI) allows rapid characterization of the 3D morphology of the developing brain using its endogenous contrast without perturbation to the tissue structure.

Diffusion tensor imaging is a new MR technique that can study the existence and orientation of "ordered structures" using the process of water diffusion as a probe (Fig. 1) (Le Bihan et al., 1986; Moseley et al., 1990; Basser et al., 1994; Beaulieu and Allen, 1994; Henkelman et al., 1994; Mori et al., 2001; Zhang et al., 2002). Specifically, the technique can measure the extent of water diffusion along an arbitrary axis (Fig. 1B). In tissue, water often tends to diffuse along a preferential axis (called diffusion anisotropy), which has been shown to coincide with the orientation of "ordered structures," such as axonal tracts (Fig. 1B and C). Diffusion

* Corresponding author. Johns Hopkins University School of Medicine, Department of Radiology, Division of MRI Research, 720 Rutland Ave., Baltimore, MD 21205, USA. Fax: +1-410-614-1948.
E-mail address: susumu@mri.jhu.edu (S. Mori).

1053-8119/$ – see front matter © 2003 Elsevier Inc. All rights reserved.
doi:10.1016/S1053-8119(03)00410-5

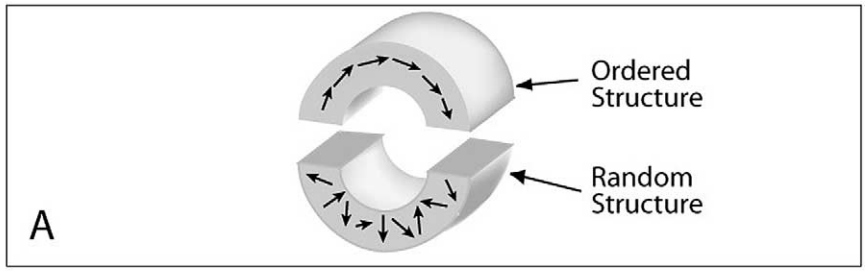
Ordered
Structure
Random
Structure
A

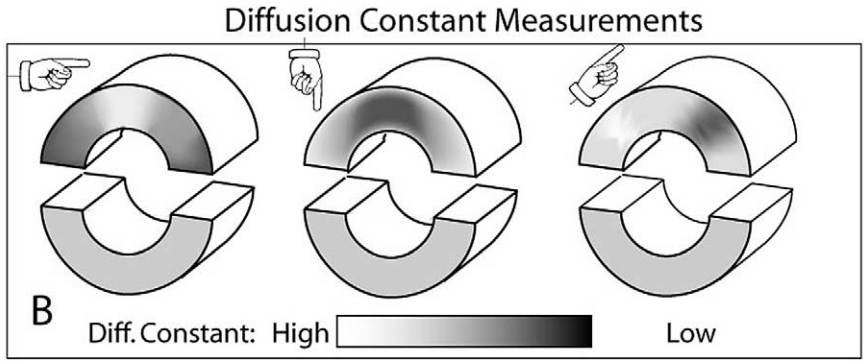
Diffusion Constant Measurements
B
Diff. Constant: High
Low

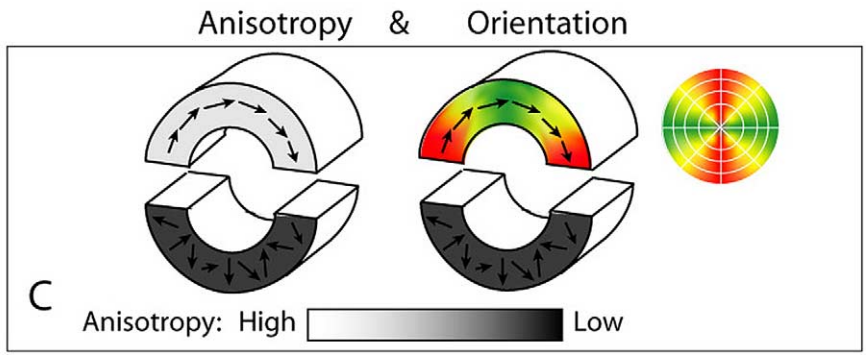
Anisotropy & Orientation
C
Anisotropy: High
Low

1

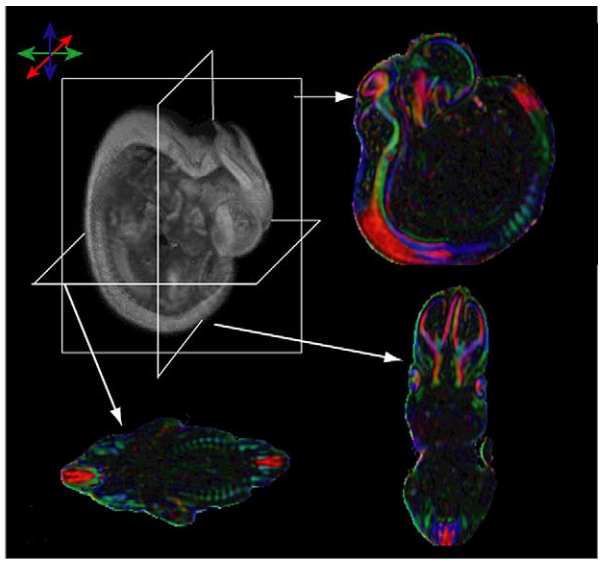

2

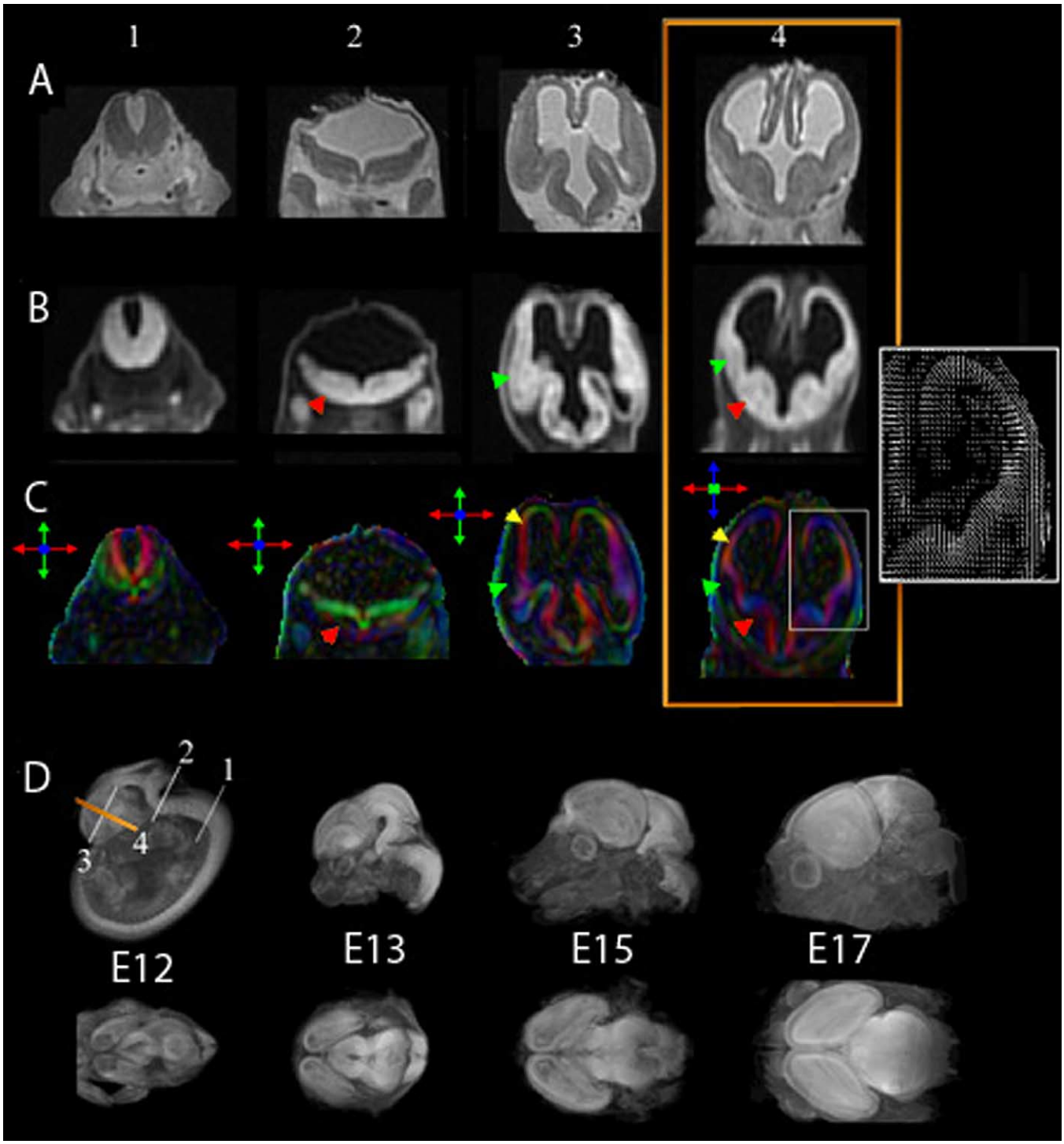

Fig. 3. Comparison between conventional T_2-weighted MRI (A), diffusion-weighted MRI (iDWI) (B), and the DTI-based color maps (C) of the E12 brains, and 3D volume rendering of mouse brains from E12 to E17 viewed from side and top of the brains (D). Images in A–C were taken from plane locations indicated in the side view of E12 in D. The color maps can differentiate the NE (yellow arrowhead) and DF such as lateral (green arrowhead) and medial (red arrowhead) ganglionic eminences. The fiber orientation of the NE can also be appreciated in the vector map of a magnified region (inset).

Fig. 1. Principles of diffusion tensor imaging. (A) A diagram of two types of brain structures. The upper region has an ordered structure due to fibers running along the arrow. The lower region has random fiber structure. (B) Apparent diffusion constant measured along the three different axes. Diffusion seems faster if the fiber orientation coincides with the measurement orientation, and becomes slower when perpendicular to it, resulting in orientation-dependent diffusion constants in the upper region. (C) Results of DTMI. Anisotropy (diffusion directionality) of the upper region is high because of the dependency on measurement orientation. When arisotropy is high, the fiber angle can be calculated based on the information in B, which can be represented by vectors or by color. In this 2D example, regions with fibers running horizontally are green and those running vertically are red. Transition areas become yellow, a mixture of green and red. Note that the technique cannot distinguish afferent and efferent axonal tracts.

Fig. 2. Color maps of E12 mouse embryo. Actual scans are performed three-dimensionally and three principal colors (red, green, blue) are assigned to one of the imaging coordinates, as shown by colored arrows. Three representative slices are extracted from the 3D data and shown.

tensor imaging can provide several imaging contrasts such as anisotropy and orientation maps (Fig. 1C), or a combination of the two, called color-coded orientation map or simply color map hereafter (Fig. 2). In color maps, the brightness reflects the extent of anisotropy, while the color represents fiber orientation. It is this color map that carries a wealth of embryonic neuroanatomical information. The goal of this study was to examine the potential of DTMI for characterization of 3D anatomical structures in developing mouse brains. We presented here the effectiveness and accuracy of DTMI for normal and abnormal brain development. Our analysis focused on the development of cortex and axonal projections, and validated our DTMI results with previous histological findings. Our technique was successfully applied in examination of anatomical phenotype of Netrin-1 knock-out mice.

Methods and materials

MR data acquisition

Specimens were fixed using 4% paraformaldehyde in phosphate-buffered saline (PBS) and stayed in fixation solution for over 1 month. Before imaging, we placed specimens in PBS for more than 24 h and transferred them into home-built MR-compatible tubes. The tubes were filled with fombin (Fomblin Profludropolyether, Ausimont. Thorofare, NJ, USA) to prevent dehydration. Imaging was performed using a GE Omega 400 (9.4 T) spectrometer. We used a custom-made solenoid volume coil as both the radio frequency (RF) signal transmitter and receiver. The NMR sequence was based on a 3D multiple echo sequence with navigator-echo phase correction scheme (Mori and van Zijl, 1998; Xue et al., 2001). Four echoes were acquired for each excitation. The first two echoes were used for imaging and the last two echoes were navigator echoes to monitor any instrumental instabilities and subsequent signal phase and intensity changes during the scan (Zhang et al., 2002). Both high-resolution T_2-weighted images and diffusion-weighted images were acquired with the same field of view [$9.5 \times 6 \times 6$ mm for the smallest sample (E 12) and $11 \times 7.5 \times 7.5$ mm for E18]. For diffusion-weighted images, the imaging matrix had a dimension of $128 \times 70 \times 72$, which was zero-filled to $256 \times 140 \times 144$ after the spectral data were apodized by a 10% trapezoidal function. For high-resolution T_2-weighted images, the imaging matrix had a dimension of $256 \times 105 \times 96$, which was zero-filled to $512 \times 209 \times 192$ after the spectral data were apodized by a 15% trapezoidal function. The pixel size after the zero-filling for E12 was $37 \times 43 \times 42$ μm for diffusion-weighted images, and $19 \times 29 \times 31$ μm for T_2-weighted images. Eight to 14 diffusion-weighted images were acquired with different diffusion gradient directions and magnitudes. For diffusion-weighted images, a repetition time (TR) of 0.9 s, an echo time (TE) of 37 ms, and two signal averages were used, for a total imaging time of 24 h. For T_2-weighted images, we used a TR of 1.8 s, a TE of 80 ms, and two signal averages for a total imaging time of 8 h.

Data processing

The diffusion tensor was calculated using a multivariate linear fitting method, and three pairs of eigenvalues and eigenvectors were calculated for each pixel. The eigenvector associated with the largest eigenvalue was referred to as the primary eigenvector. For the quantification of anisotropy, fractional anisotropy (FA) was used (Pierpaoli and Basser 1996). Isotropic diffusion-weighted images (iDWI) were the sum of diffusion-weighted images with different diffusion gradient directions. Using primary eigenvector and FA, color maps were calculated. In the color map images, the R(ed), G(reen), and B(lue) value of each pixel was defined by the orientation of its primary eigenvector, and the intensity was proportional to the FA. Red was assigned to the fiber orientation along the anterior-posterior axis, green to the right-left axis, and blue to the dorsal-ventral axis.

We used a multiple region or interest (ROI) approach to delineate neuronal fibers based on our tensor data. In the beginning, we placed several ROIs along the possible path of a fiber track. We then used FACT algorithm (Mori et al., 1999; Xue et al., 1999) to find any fiber that passed through all these ROIs (Conturo et al., 1999; Stieltjes et al., 2001). This approach utilized prior knowledge of the orientation and path of existing neuronal fibers derived from existing histological studies.

Results

Fig. 2 shows color maps at three orthogonal cross sections of an embryonic day 12 (E 12) mouse embryo. At this stage, central nervous system, including telencephalic wall, diencephalon, spinal cord, and so on, showed a high degree of diffusion anisotropy. Fig. 3 shows comparison between conventional T_2-weighted (Fig. 3A), diffusion-weighted (Fig. 3B), and color maps (Fig. 3C) of an E12 mouse brain at several locations. In Fig. 3D, we demonstrated 3D volume renderings of E12 to E17 mouse brains to show how telencephalic vesicles ballooned dorsally and laterally to cover diencephalons. Conventional T_2-weighted images and diffusion-weighted images could only identify the central nervous system (CNS) as a homogeneous structure, and fail to provide anatomical detail within it. The color map, on the contrary, can distinguish many internal structures. For example, at E12, the telencephalon and diencephalon are made up of two regions, i.e., the neuroepithelium (NE) where neurons are born, and differentiating fields (DFs) where neurons migrate from the NE and start to differentiate. These two regions can be distinguished by the color maps. The NE has high anisotropy (bright, indicated by

yellow arrowheads) due to the orderly arrangement of radial glia and proliferating cells whose orientation is perpendicular to the ventricle (see the vector map in the inset). The DFs are less organized and have a low anisotropy. In the following sections, we will introduce how the dynamics of the gray and white matter formation can be delineated using the DTMI.

Cortical development under DTMI

During CNS development, neurons are born in the NE surrounding the ventricle. They then differentiate and form axons to communicate with other neurons. As a result, many regions of the CNS have a neurons inside (gray matter is closer to the ventricle)–axons outside (white matter is closer to the pial surface of the CNS) configuration. One notable exception is the cerebral cortex, in which the gray matter lies outside the white matter. This gray matter–white matter inversion occurs during E12–18 in the mouse, when neurons born in the NE migrate outward along radial glia and detach to form the layers of the cortical plate in an inside-out fashion (Rakic, 1972). Fig. 4A shows how this inversion process can be visualized by DTMI. The NE is the only structure with a high anisotropy at E12 (blue arrowhead). At E13–14, two more structures with high anisotropy emerge, the cortical plate (CP) and the intermediate zone (IZ, axonal tracts). The CP (indicated by pink arrowheads) arises first in the ventrolateral portion of the dorsal telencephalon and extends anteriorly and dorsomedially during development. It has the same fiber orientation (color) as the NE and its appearance is followed by a drastic reduction in the NE below (see diagram and color maps in the inset). The anterior and dorsomedial front of the emerging CP also coincides with the growing axonal tracts (IZ, its leading edge is indicated by yellow pins). Unlike the NE and CP, which have fiber orientations perpendicular to the ventricular surface, the orientation of the IZ is always parallel to the surface, as can be seen from the color and vector maps shown at E16 (Fig. 4A). By E17, medially projecting cortical axons within the IZ penetrate the midline, forming the corpus callosum. This inversion process can be easily viewed even within one single brain at E14 or E15 because of the lateral-medial developmental gradient.

Development of axonal tracts

Using DTMI, axonal tracts can be identified due to their high anisotropy and characteristic fiber orientation. For example, Fig. 4C shows midsagittal images during E15–18, in which commissural tracts can be readily identified (tract orientation is perpendicular to the imaging plane represented by green). At E15, the optic chiasm (white arrowheads) is the only commissural fiber that penetrates the midline. At E16, the hippocampal commissure (yellow) and anterior commissure (pink) cross the midline, although the anterior commissure appears faint. By E17 and E18, the anterior commissure and hippocampal commissure increase in size and a portion of the corpus callosum emerges (blue arrowheads).

3D characterization of brain development

One of the benefits of scanning postmortem samples using MRI, rather than or in addition to histological processing, is that DTMI provides an efficient and accurate means for 3D anatomical analyses. For example, Fig. 4B shows the emerging CP, which originates at the lateral regions, extends toward the midline, and by E16 covers the entire hemisphere, while at the same time becoming thicker from midanterior areas. Cortical thickness measurements cannot be easily achieved by 2D-based histology because most predetermined slices contain cortical areas that are sliced obliquely, resulting in a thickness that seems artificially thick.

Fig. 5A shows examples of 3D segmentation of E12 embryo. In the first step, the ventricle and the entire CNS can be delineated using conventional MRI such as T_2W images. The CNS can be further divided into the NE and DF based on DTMI analysis. Fig. 5B shows how each region changes shape during development. It can be clearly seen how the space that originally belongs to ventricle and NE are gradually occupied by DFs (gray matter nuclei). Three-dimensional trajectories of axonal tracts can also be reconstructed using DTMI data. Fig. 5C shows the projection of thalamocortical projection (tcp, white) and stria terminalis (st, orange), one of the earliest formed white matter tracts that connects thalamus–CP (tcp) or hypothalamus/septum–amygdala (st). The figure clearly shows geometrical relationships between different axonal tracts and/or between tracts and gray matter neclei. Using this technique, it is now possible to study the emergence and morphological changes of prominent white matter tracts in relation to one another during development as well as in cases displaying brain abnormalities.

An example of phenotypic characterization using DTMI

As mentioned above one of the great advantages of using DTMI is the capability to do rapid whole-brain phenotype analysis of mutant strains. Further histological analysis can then be targeted to precise regions of the brain or specific fiber tracts. In the Netrin-1 mutant, most of the major midline commissures within the brain are missing (Serafini et al., 1996). We examined embryonic day 17 Netrin-1 mutant brains to determine whether commissural defects known to occur in these animals could be detected using DTMI. Fig. 6A compares color maps and T_2Ws of midsagittal planes of a Netrin-1 mutant mouse (KO) and a wild-type littermate (WT). From the T_2Ws, it is difficult to identify specific differences between the two mice. However, using the color maps, it is evident that the Netrin-1 mutant lacks a corpus callosum, anterior commissure, and a

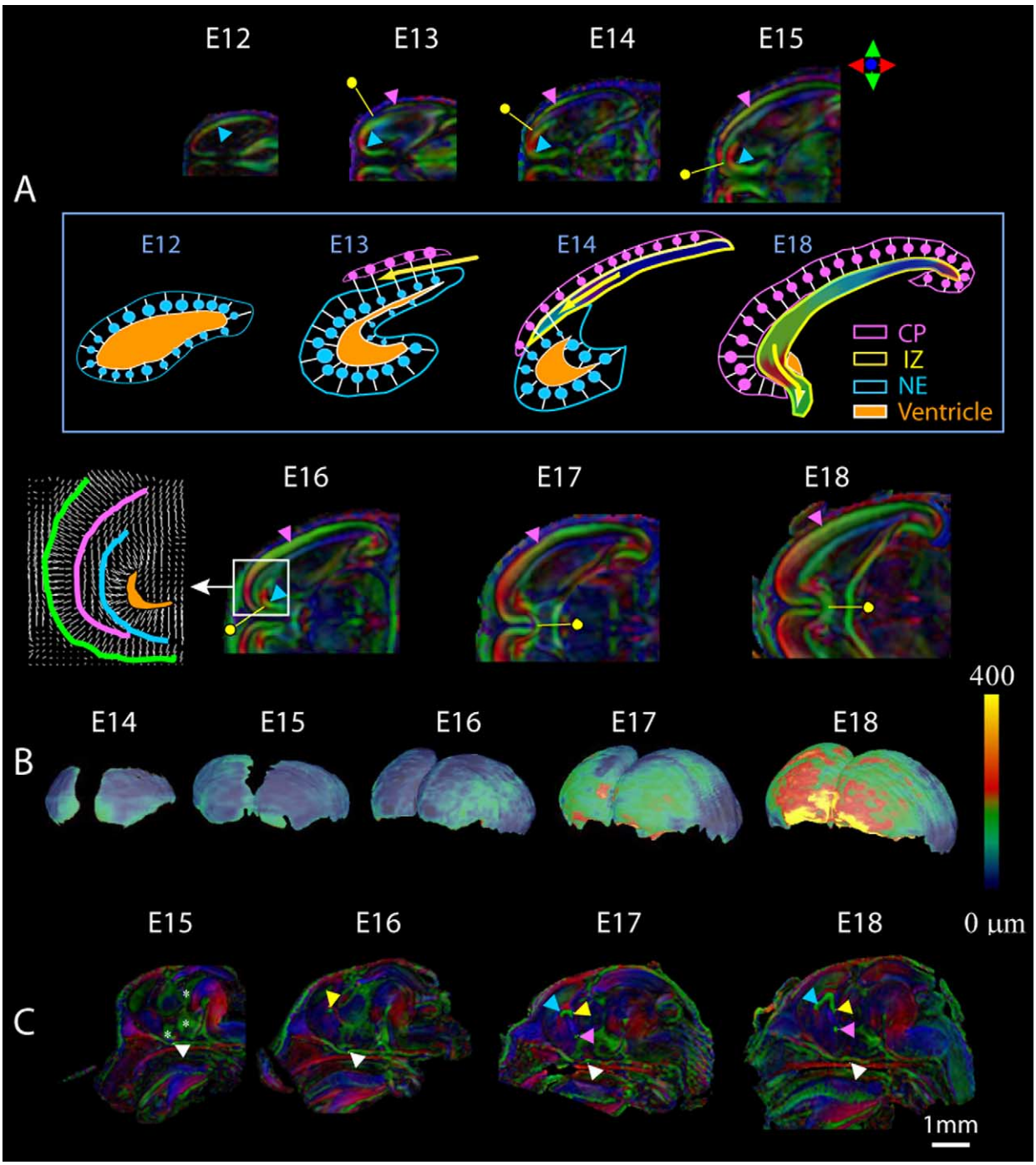

Fig. 4. Cortical and white matter development. (A) Horizontal planes of color maps of E12–18 brains. Blue and pink arrowheads indicate locations of the NE and CP. Yellow pins indicate the leading edge of the growing IZ (axonal tracts) in between the NE and CP. The inset diagram explains the cellular events during E12–18 based on radial migration theory. Blue circles indicate newly born neurons in the NE, white bars represent migration scaffolds by the radial glia, pink circles are neurons in the CP, and yellow arrows are the growing axons. At E12, there is only one layer (NE), which has radial structures around the ventricle. At E13, the CP emerges and simultaneously afferent and efferent axons (IZ) arrive between the NE and CP layers, resulting in a temporary three-layer structure. At E14–18, the CP formation progressively completes with concomitant loss of the NE layer and ventricle shrinkage, while the axons follow the leading edge of the CP. A portion of E16 brain (white box) is enlarged to show the fiber orientation in a vector picture. (B) Changes in three-dimensional volumes and thickness of the CP over the period of E14–18. The volumes were hand-segmented and thickness of the volumes normal to the brain surface were measured. (C) White matter development shown at midsagittal levels of E15–18 brains. The commissural tracts can be identified by the green color. Arrowheads, optic chiasm; yellow, hippocampal commissure; pink, anterior commissure; blue, corpus callosum. Intense green structures indicated by asterisks are NE around the walls of the third ventricle.

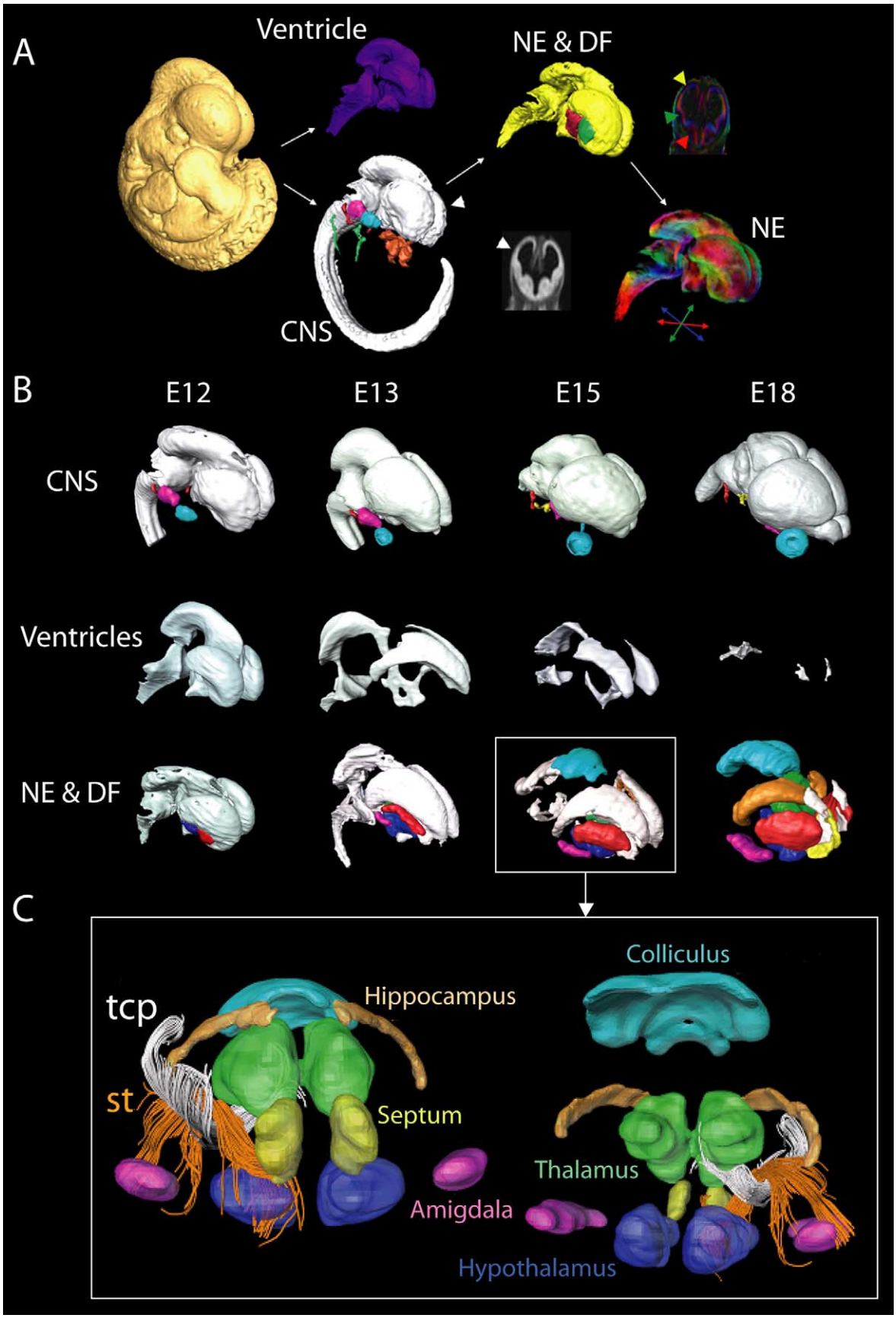
A
Ventricle
NE & DF
NE
CNS
B
E12
E13
E15
E18
CNS
Ventricles
NE & DF
C
tcp
st
Hippocampus
Septum
Amigdala
Colliculus
Thalamus
Hypothalamus

hippocampal commissure (Fig. 6A and B). Furthermore, not only was the absence of fiber tracts detected, but the absence of several gray matter structures is also evident using this technique. In Netrin-1 mutants the basilar pons fails to form due to defects in the migration of cells from the rhombic lip that give rise to this structure (Yee et al., 1999). A comparison of the Netrin-1 mutant brain with a wild-type littermate clearly shows an absence of the basilar pons in the mutant (Fig. 6A and C). These results show that DTMI can be used to detect gross anatomical defects in mutant brains and can provide an effective preliminary screen for such brains prior to further histological analysis.

Discussion

Our study demonstrates the effectiveness of DTMI in characterizing the global architecture of developing neuroanatomy. Compared to other imaging modalities, the MR-based technique has two significant limitations, namely imaging resolution and contrast. In this study, we achieved an imaging resolution of up to 80 μm. In the future, due to the recent advent of microimaging techniques (Johnson et al., 1997; Jacobs et al., 1999), a resolution of 10–20 μm should be possible, although this still cannot match the resolution of optical techniques and, therefore, imaging of cellular level anatomy is difficult with this technique. However, MRI still has major advantages over conventional histological techniques. Conventional histology has a lower resolution along the slice orientation (typically 10–50 μm) and usually has information gaps unless hundreds of perfect and contiguous slices are obtained, which is painstaking and often not practical. In many cases, information about an entire brain is extrapolated from a limited number of histological slices for volumetric studies. As a result, histology-based studies do not always convey proficient resolution in 3D for the entire brain.

More significant limitations of conventional MR stem from a lack of anatomical contrasts. Similar to the fact that unstained histological preparation is of limited value, the usefulness of MR images hinges on its power to provide contrasts for differentiating various anatomical units. As shown in Figs. 3 and 6, conventional MR images have poor contrast in embryonic brains mainly due to the lack of myelination. Here, DTMI is a breakthrough because it can provide rich anatomical information in embryonic brains based on orientation information. Our study indicates that the DTMI can identify various early brain structures including the NE, DF, and CP without perturbing the tissue. The capability of DTMI to discretely identify these structures without sectioning and chemical staining is unmatched by any existing imaging modalities. It can also delineate trajectories of certain white matter tracts, which may be difficult even with digitally reconstructed 3D histological data.

Compared to histological examination, MRI excels in surveying the entire brain in an unbiased fashion to detect abnormalities, which can arise due to gene alterations, pharmacological treatments, or induced lesions. Histology often requires assumptions about a possible phenotype prior to analysis so that the optimal plane of section and the selection of appropriate stains or antibodies to visualize specific structures can be chosen. These prior assumptions can cause some phenotypical changes to be overlooked, or require large numbers of mutant animals to analyze several possible phenotypes. Since DTMI can examine the entire brain in an efficient and possibly more quantitative manner, it provides an excellent broad analysis of the phenotype, which can then be followed by more detailed histological analyses of the appropriate regions. The same brain that is used for DTMI analysis can be used subsequently for more detailed histological analysis.

The dynamics of cortical development revealed by this technique supports the radial migration theory of cortical neurons (Rakic, 1972; Nadarajah and Parnavelas, 2002). In addition to the delineation of normal brain development processes, DTMI could provide an efficient and accurate means for anatomical characterization of mutant phenotypes such as the Netrin-1 mutant described here. Another potential application of DTMI would be for coregistration studies with gene expression stains based on other imaging modalities such as histological sectioning (Streicher et al., 2000; Weninger and Mohun, 2002), followed by in situ hybridization or antibody labeling, MRI with contrast agents (Louie et al., 2000), and optical projection tomography (Sharpe et al., 2002), which can detect the location of different gene expression patterns in the 3D space but often lacks contrast to delineate the underlying anatomy.

In this study, we scanned at least two samples at each developmental time point. In this study, however, for qualitative description of brain development, we showed images from only one embryo at each time point. One of the most important unanswered questions is confidence level of the

Fig. 5. Three-dimensional segmentation of the CNS. (A) Segmentation scheme using an E12 embryo. The ventricle and CNS were segmented using conventional MRI microscopy. Several cranial nerves are also identified and painted as brown (nasal nerve), blue (optic nerve), pink (V), red (VII), and green (IX, X). The NE (yellow) and DF (red and green) were then segmented using the color map. The NE with color presentation for the glial orientation is also shown. (B) Evolution of each 3D segment during the brain development. Note that the ventricle has a similar shape as the CNS at E-12, but it shrinks dramatically during the development, which is replaced by the DF. The color coding of the DF is as follows: red, caudoputamen; yellow, septum; pink, amygdala; orange, hippocampus; blue, hypothalamus; green, thalamus; light blue, colliculus. Because of the difficulties to precisely identify the boundaries of these gray matter structures, only the cores were defined. (C) Three-dimensional reconstruction of thalamocortical projection (tcp, white) and stria terminalis (st, orange) at E15. For clear presentation, the NE (white) and the caudoputamen (red) were removed. For the 3D reconstruction, fiber assignment by continuous tracking (FACT) was used (Mori et al., 1999; Xue et al., 1999).

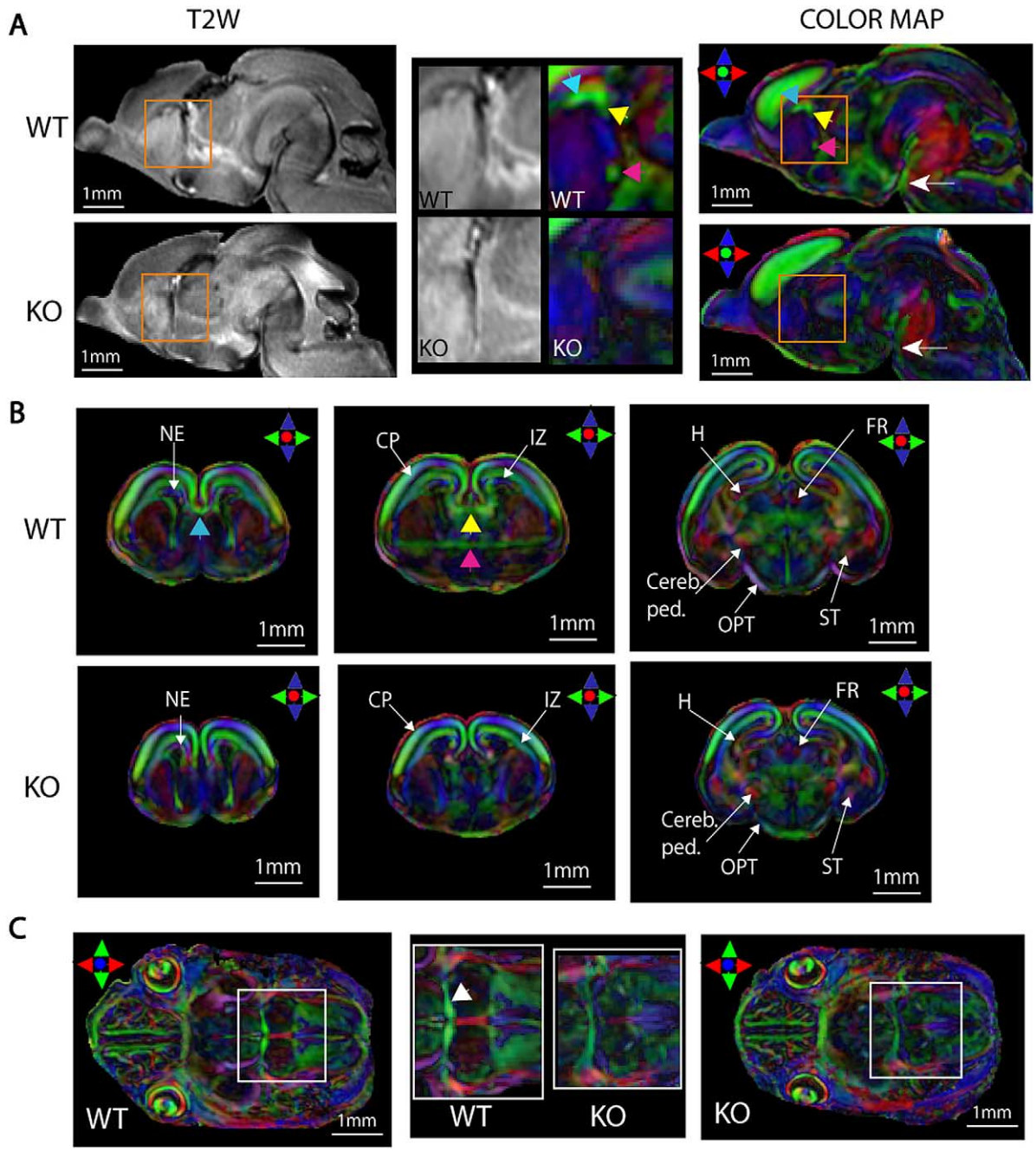

Fig. 6. Comparison between Nutrin-1 mutant mouse and a littermate at E17. Structures that were selectively missing are indicated by arrowheads. These are corpus callosum (blue arrowhead), hippocampal commissure (yellow), and anterior commissure (pink). The cortical formation (CP, IZ, and NE), hippocampus, and other noncommissural tracts were well preserved. Abbreviations: H, hippocampus; Cereb. Ped., cerebral peduncle; OPT, optic tract; ST, stria terminalis; FR, fasciculus retrofrexus.

MRI observation of developing brains. To answer this question, we need many more numbers of samples at each time point and sophisticated shape analysis tools to characterize normal individual variations. Application of latest techniques of computational neuroanatomy, mostly developed for human brain studies, to this type of data set may prove to be important and exciting in the future.

This study was based on ex vivo tissues. In vivo MR-DTMI of embryos is at present difficult due to the long scanning time required and motion stabilization issues. Another drawback of the current DTMI technique is the length of the scan (16–24 h in this study). With the spatial resolution used here, the signal-to-noise ratio of raw images was more than 40, and the imaging time was restricted by the number of phase-encoding steps (more than 3600 steps). In the future, the implementation of rapid imaging techniques that allow for the fast acquisition of multiple phase-encoded images will effectively shorten the scanning time.

In conclusion, DTMI provides superb contrast that enables the observation of various structures within embryonic brains and excels in the global characterization of development processes. Critical anatomical regions, such as the NE, DF, cortical plate, and various axonal tracts, were reconstructed in 3D. The technique was applied to the Netrin-1 mutant mouse model, which clearly showed abnormalities in most of the major midline commissures. The MR scans do not impede the subsequent histological processing of the tissue, so the same sample can be processed using both techniques. By combining macroscopic DTMI analysis with follow-up histological analysis, a more sensitive and efficient collection of relevant anatomical data should be possible.

Acknowledgments

This study was supported by NIH grants RO1 AG20012-01, RO3 HD41407-01A1, and P41 RR15241-01. We thank Kimberly M. Valentino and Celine Plachez for help in preparing brain specimens.

References

Basser, P.J., Mattiello, J., Le Bihan, D., 1994. MR diffusion tensor spectroscopy and imaging. Biophys. J. 66, 259–267.

Beaulieu, C., Allen, P.S., 1994. Determinants of anisotropic water diffusion in nerves. Magn. Reson. Med. 31, 394–400.

Boppart, S.A., Bouma, B.E., Brezinski, M.E., Tearney, G.J., Fujimoto, J.G., 1996. Imaging developing neural morphology using optical coherence tomography. J. Neurosci. Methods 70, 65–72.

Conturo, T.E., Lori, N.F., Cull, T.S., Akbudak, E., Snyder, A.Z., et al., 1999. Tracking neuronal fiber pathways in the living human brain. Proc. Natl. Acad. Sci. USA 96, 10422–10427.

Henkelman, R., Stanisz, G., Kim, J., Bronskill, M., 1994. Anisotropy of NMR properties of tissues. Magn. Reson. Med. 32, 592–601.

Jacobs, R.E., Ahrens, E.T., Dickinson, M.E., Laidlaw, D., 1999. Towards a microMRI atlas of mouse development. Comput. Med. Imaging Graph. 23, 15–24.

Jacobs, R.E., Ahrens, E.T., Meade, T.J., Fraser, S.E., 1999. Looking deeper into vertebrate development. Trends Cell. Biol. 9, 73–76.

Jacobs, R.E., Fraser, S.E., 1994. Imaging neuronal development with magnetic resonance imaging (NMR) microscopy. J. Neurosci. Methods 54, 189–196.

Johnson, G.A., Benveniste, H., Black, R.D., Hedlund, L.W., Maronpot, R.R., et al., 1993. Histology by magnetic resonance microscopy. Magn. Reson. Q. 9, 1–30.

Johnson, G.A., Benveniste, H., Engelhardt, R.T., Qiu, H., Hedlund, L.W., 1997. Magnetic resonance microscopy in basic studies of brain structure and function. Ann. NY Acad. Sci. 820, 139–147.

Le Bihan, D., Breton, E., Lallemand, D., Grenier, P., Cabanis, E., et al., 1986. MR imaging of intravoxel incoherent motions: application to diffusion and perfusion in neurologic disorders. Radiology 161, 401–407.

Louie, A.Y., Huber, M.M., Ahrens, E.T., Rothbacher, U., Moats, R., et al., 2000. In vivo visualization of gene expression using magnetic resonance imaging. Nat. Biotechnol. 18, 321–325.

Mori, S., Crain, B.J., Chacko, V.P., van Zijl, P.C.M., 1999. Three dimensional tracking of axonal projections in the brain by magnetic resonance imaging. Ann. Neurol. 45, 265–269.

Mori, S., Itoh, R., Zhang, J., Kaufmann, W.E., van Zijl, P.C.M., et al., 2001. Diffusion tensor imaging of the developing mouse brain. Magn. Reson. Med. 46, 18–23.

Mori, S., van Zijl, P.C.M., 1998. A motion correction scheme by twin-echo navigation for diffusion weighted magnetic resonance imaging with multiple RF echo acquisition. Magn. Reson. Med. 40, 511–516.

Moseley, M.E., Cohen, Y., Kucharczyk, J., Mintorovitch, J., Asgari, H.S., et al., 1990. Diffusion-weighted MR imaging of anisotropic water diffusion in cat central nervous system. Radiology 176, 439–445.

Nadarajah, B., Parnavelas, J.G., 2002. Modes of neuronal migration in the developing cerebral cortex. Nat. Rev. Neurosci. 3, 423–432.

Pierpaoli, C., Basser, P.J., 1996. Toward a quantitative assessment of diffusion anisotropy. Magn. Reson. Med. 36, 893–906.

Rakic, P., 1972. Mode of cell migration to the superficial layers of fetal monkey neocortex. J. Comp. Neurol. 145, 61–83.

Serafini, T., Colamarino, S.A., Leonardo, E.D., Wang, H., Beddington, R., et al., 1996. Netrin-1 is required for commissural axon guidance in the developing vertebrate nervous system. Cell 87, 1001–1014.

Sharpe, J., Ahlgren, U., Perry, P., Hill, B., Ross, A., et al., 2002. Optical projection tomography as a tool for 3D microscopy and gene expression studies. Science 296, 541–545.

Stieltjes, B., Kaufmann, W.E., van Zijl, P.C.M., Fredericksen, K., Pearlson, G.D., et al., 2001. Diffusion tensor imaging and axonal tracking in the human brainstem. NeuroImage 14, 723–735.

Streicher, J., Donat, M.A., Strauss, B., Sporle, R., Schughart, K., et al., 2000. Computer-based three-dimensional visualization of developmental gene expression. Nat. Genet. 25, 147–152.

Weninger, W.J., Mohun, T., 2002. Phenotyping transgenic embryos: a rapid 3-D screening method based on episcopic fluorescence image capturing. Nat. Genet. 30, 59–65.

Xue, R., Sawada, M., Goto, S., Hurn, P.D., Traystman, R.J., et al., 2001. Rapid three-dimensional diffusion MRI facilitates the study of acute stroke in mice. Magn. Reson. Med. 46, 183–188.

Xue, R., van Zijl, P.C.M., Crain, B.J., Solaiyappan, M., Mori, S., 1999. In vivo three-dimensional reconstruction of rat brain axonal projections by diffusion tensor imaging. Magn. Reson. Med. 42, 1123–1127.

Yee, K.T., Simon, H.H., Tessier-Lavigne, M., O'Leary, D.M., 1999. Extension of long leading processes and neuronal migration in the mammalian brain directed by the chemoattractant netrin-1. Neuron 24, 607–622.

Zhang, J., van Zijl, P.C., Mori, S., 2002. Three dimensional diffusion tensor magnetic resonance micro-imaging of adult mouse brain and hippocumpus. NeuroImage 15, 892–901.